Performance Enhancement of DFIG Based Grid Connected SHPP Using ANN Controller

Sanjeev Kumar Gagrai*, Sundram Mishra**‡, Madhu Singh***

* Department of Electrical Engineering, NIT, Jamshedpur (831014), Jharkhand, India

** Department of Electrical Engineering, NIT, Jamshedpur (831014), Jharkhand, India

*** Department of Electrical Engineering, NIT, Jamshedpur (831014), Jharkhand, India

(sanjeev.mit03@gmail.com, sundram79808183@gmail.com , madhu.ee@nitjsr.ac.in)

‡Corresponding Author; Sundram Mishra, Department of Electrical and Electronics Engineering, NIT, Jamshedpur (831014), Jharkhand, India, Tel: 9354701980, sundram79808183@gmail.com

Received: 18.04.2019 Accepted: 08.06.2019

Abstract- In the current span of time, Small Hydro Power Plant (SHPP) is gaining more attention due to its numerous pros among all the various renewable energy sources. The prime objective of this paper to present the comparative analysis of Proportional Integral (PI)control and Artificial neural network (ANN) control strategy which is used in doubly fed induction generator based SHPP. Traditionally presented PI control scheme has numerous limitations due to nonlinear model of DFIG, as well as PI control scheme, needs plentiful mathematical equations. To significantly improve transient response of DFIG system as well as reduce the computational time of the system, ANN control scheme is implemented in rotor side and grid side of the small hydro power plant system. The proposed ANN scheme significantly improves the transient behaviour of active and reactive power in rotor side and reactive power and dc bus voltage in grid side as compare to PI control scheme. MATLAB/SIMULINK is used for testing, analysing and comparison of dynamic and steady state realization of proposed controller scheme. The stability of the system is constant under various load circumstances and it is scrutinized with the help of model and simulated results.

Keywords- Small Hydro Power Plant, Rotor side control, Grid side control, Comparison, Proportional Integral Control, Artificial Neural Network control.

1. Introduction

In less than another 10 decades, the fossil-based fuels, natural gases, and oil will be exhausted according to prediction of the World Energy Forum. Fossil-based fuels are responsible for 79% of primary energy consumption in all over world and 58% of that amount is used in transport sector, that's why it is diminishing swiftly [1]. In the current epoch of time, electric power industry is facing numerous serious problems like as limited conventional energy sources, environmental protection and day by day increment of energy consumption [1, 2]. The inadequacy of fossil fuels and its effects on the climate change increasing the demand of renewable energy sources especially small hydro power plant. As SHPP is highly suitable for remote areas with less capital cost. According to Ministry of New and Renewable Energy (MNRE), India is about generate 175000 MW of total nonconventional energy capacity by 2022 [2, 8]. This 175000 MW includes 5000 MW small hydro projects so the development of SHPP is very much important [3]. Among all the renewable energy sources, hydro power is gaining more attention nowadays. According to "BP Statistical Review of World Energy, 22 % of worldwide power generation procure from hydropower. The system is known as hydroelectric energy system which are used to extracting the electricity from water. In numerous countries, 3673 Terawatt-hours of energy are consumed from hydropower [3, 4].

DFIG has attained the massive consideration over the last decade due to its ample of gains in variable speed application [5]. DFIG became very much popular in wind energy utilization due to inconstant speed of the wind. So the main originality of this research work is the use of DFIG in the SHPP because in SHPP we can generate electricity from the running water so we do not need reservoir for storing the water. DFIG offers a lot of benefits such as regulation of the torque, significantly increase the flow of real power from rotor side to grid side and reducing the expenditure of power electronics converter [6]. Basically, DFIG significantly improves the statbilty performance of the system in the low

speed as well as high speed operation. The reciprocating span of time of the DFIG is very much less throughout the demanding of the active and reactive power in the network. In the course of grid failure, the DFIG reactive power injection that receipts place using the crowbar circuit to function deprived of detaching from the network [5, 6,7, 8].

The power transmitted between the DFIG's stator side and electrical grid independently controlled by the vector control orientation which is applied to stator field [9]. During the last decade, numerous control strategies have been elaborated and employed to attain the superior performance of the controlled system [10].In this research work firstly authors proposed PI controller in rotor side and grid side for controlling the active and reactive power and DC bus voltage [10, 11]. Undoubtedly PI controller gave suitable performance in rotor and grid side but along this, it grieves from sundry limitations such as nonlinearity of the DFIG model and variations in the machine parameters.

As the most parts of hydro power conversion system are nonlinear like as turbine, DFIG so the traditional PI controller is not very much suitable here [9]. In order to conquer the confines of PI controller, a newly advanced control

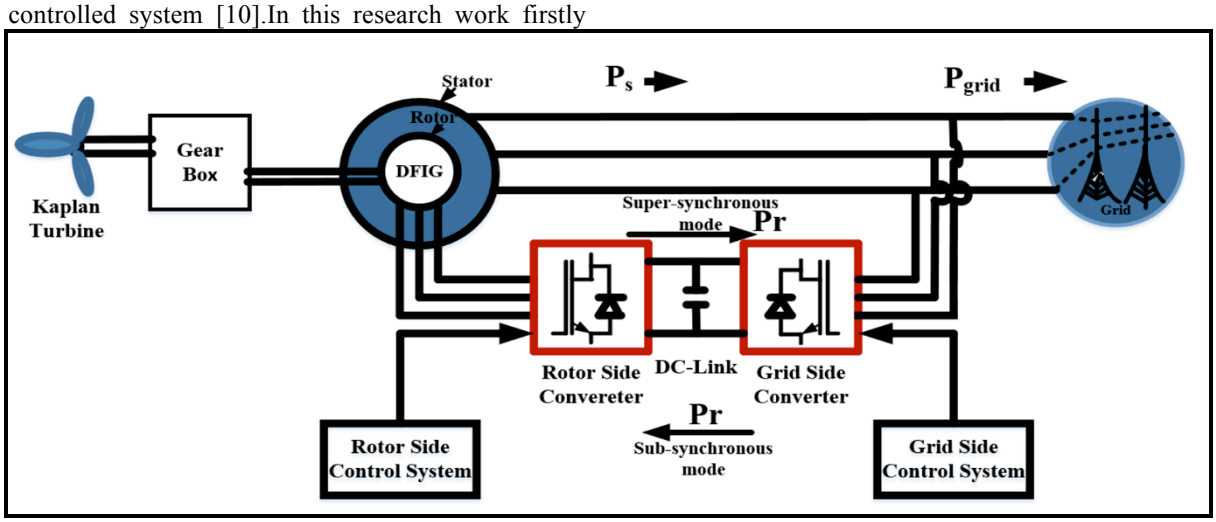

Fig. 1. Schematic representation of DFIG based SHPP system

scheme i.e. Artificial neural network control is presented here. ANN controller has plenty of advantages which improves the performance of rotor side and grid side parameters [12]. The processing of the ANN becomes very simple due to the reduction of computational complication as well as ANN-based controller improves the transient performance of the DFIG. Using the ANN approach this research work realizes real-time optimization because the optimization of this controller is done in real-time according to various real points [13]. A lot of research work has been done in wind energy application with DFIG but the implementation of DFIG in SHPP with the advanced controller like ANN will present the high innovation of the research work and this is the prime motive of this research study. In the real time application, most of the problems are highly nonlinear in nature so for that persistence we prerequisite nonlinear computational techniques such as Artificial Neural Network control scheme. This nonlinearity is distributed throughout same as in ANN all the artificial neurons are distributed throughout. it is also embracing the input-output mapping attributes [13].

The rest section of this research study is organized as follows: section 2 presents layout of the small hydro power plant associated with DFIG and back to back voltage source converter. The dynamic mathematical modelling of DFIG is presented in section 3. Section 4 represents the rotor side and grid side control scheme with PI and ANN controller. Simulation results and discussion are presented in the section 5. At last research work is completed by the conclusion.

2. Hydro Power Conversion System Description

Because of perceptible attributes such as variable speed operation, less noise, reduced mechanical stress, and superior power quality performance, the hydraulic turbine with DFIG have long been favoured choice for hydro power conversion [14]. Figure 1 represents the schematic diagram of modern DFIG based SHPP system. The hydraulic turbine which has been used here is kaplan turbine because kaplan turbine is very much suitable for low head operation (less than 10 metre) as well as it has highest efficiency (90%). The kaplan turbine is coupled with the rotor of DFIG via gear box for allowing the various level of speed amid the turbine and rotor [14, 15, 16]. For connecting the variable frequency to the grid frequency, the usefulness of power electronics is very important due to existence of variable speed and variable frequency [17]. Hence, this Voltage source inverter with PWM method aids to expand the performance in the stabilization of frequency, compensation of the reactive power and voltage regulation. Likewise, the Pulse Width Modulation strategy is implemented to eradicate voltage induced in the shaft affected by the effect of parasitic coupling under high frequency [18]. The stator body of the DFIG is directly coupled to the grid as well as rotor of DFIG is also coupled to the grid but through AC/DC/AC (bidirectional) power electronics converter. Basically, these converter is back to back voltage source inverter which is signified the rotor side converter and grid side converter.

These converters are based forced commutated IGBTs [19]. For link the DC side of both inverters as well as operated as a DC voltage source, the capacitor is used. The blades of kaplan turbine altered the mechanical power of variable flowing water and this mechanical is fed to the generator, which altered the mechanical power to electrical power and this electrical power is fed to the grid. The power flow amid rotor and the grid is known as slip power which is totally dependent on the value of slip [20, 21, 22]. When the generator operates in sub-synchronous speed, the direction of power flow is from the grid to the rotor whereas in the super -synchronous the direction of power flow from the rotor to the grid [23]. The control system of DFIG based SHPP system has to produce double signals in order to regulate the electrical power amid the kaplan turbine and grid. The initial one is used for rotor side converter to control the real and reactive power and another one is used for grid side converter for controlling the DC bus voltage at a constant and keep the reactive at a zero level for unity power factor operation [24]. Likewise, the adjustable speed operation in enhanced generation contributes greater revenues, decoupled quick active and reactive power regulation, superior grid stability, grid frequency control, and high quality power regulation. Lastly, the variable speed power plant does not requisite any power system stabilizer [25, 26].

3. DFIG Modeling

Basically, Park transformation is used for conversing the three-phase stator and rotor voltages to direct and quadrature generator model. The first step for building the model is the mathematical expressions of wound rotor induction machine in which static, as well as dynamic responses, are taken into explanation. The voltage expressions of the rotor and stator of the Doubly-fed Induction Generator (DFIG) in the arbitrary reference frame are presented below in Eq. (1) and Eq. (2) as matrix configuration [26] .

$$\begin{bmatrix} v_{ds} \\ v_{qs} \end{bmatrix} = R_s \begin{bmatrix} 1 & 0 \\ 0 & 1 \end{bmatrix} \begin{bmatrix} i_{ds} \\ i_{qs} \end{bmatrix} + \frac{d}{dt} \begin{bmatrix} \psi_{ds} \\ \psi_{qs} \end{bmatrix} + \omega_e \begin{bmatrix} 0 & -1 \\ 1 & 0 \end{bmatrix} \begin{bmatrix} \psi_{ds} \\ \psi_{qs} \end{bmatrix} \quad (1)$$

$$\begin{bmatrix} v_{dr} \\ v_{qr} \end{bmatrix} = R_r \begin{bmatrix} 1 & 0 \\ 0 & 1 \end{bmatrix} \begin{bmatrix} i_{dr} \\ i_{qr} \end{bmatrix} + \frac{d}{dt} \begin{bmatrix} \psi_{dr} \\ \psi_{qr} \end{bmatrix} + (\omega_e - P\omega_r) \begin{bmatrix} 0 & -1 \\ 1 & 0 \end{bmatrix} \begin{bmatrix} \psi_{dr} \\ \psi_{qr} \end{bmatrix} \quad (2)$$

Due to misalignment fields of the rotor and stator flux, the torque is generated in DFIG. So the electromagnetic torque can be represented in the Eq. (3) in the form of direct and quadrature axis stator and rotor flux and currents [21,25]:

$$T_e = 0.75P \begin{bmatrix} \psi_{ds} & \psi_{qs} \end{bmatrix} \begin{bmatrix} i_{qs} \\ -i_{ds} \end{bmatrix} \quad (3)$$

Where:

r, s = Indices of rotor and stator

i, v, ψ = Current, voltage and flux linkages of DFIG in arbitrary reference frame

Rs, Rr =Resistances of stator and rotor

Ls, Lr = Self inductances of stator and rotor

Lm = Inductance which linkage between stator and rotor.

ω_e, ω_r = Speed of the reference frame and the rotor

Te = Electromagnetic torque

P = No. of poles

The expressions of flux linkage of the DFIG in matrix configuration are given below in Eq. (4) and Eq. (5) by taking the assumptions of linearization of magnetic circuit which is used in DFIG and equal values of mutual inductance. Along this core loss is also neglected [26]:

$$\begin{bmatrix} \psi_{ds} \\ \psi_{qs} \end{bmatrix} = L_s \begin{bmatrix} I \end{bmatrix} \begin{bmatrix} i_{ds} \\ i_{qs} \end{bmatrix} + L_m \begin{bmatrix} I \end{bmatrix} \begin{bmatrix} i_{dr} \\ i_{qr} \end{bmatrix} \quad (4)$$

$$\begin{bmatrix} \psi_{dr} \\ \psi_{qr} \end{bmatrix} = L_m \begin{bmatrix} I \end{bmatrix} \begin{bmatrix} i_{ds} \\ i_{qs} \end{bmatrix} + L_r \begin{bmatrix} I \end{bmatrix} \begin{bmatrix} i_{dr} \\ i_{qr} \end{bmatrix} \quad (5)$$

Where:

$L_s = L_m + L_{ls}$, $L_r = L_m + L_{lr}$

$$\begin{bmatrix} I \end{bmatrix} = \begin{bmatrix} 1 & 0 \\ 0 & 1 \end{bmatrix}$$

From the previous flux linkages expressions, we can get current expressions by applying inverse matrix laws as shown in Eq. (6) and Eq. (7).

$$\begin{bmatrix} i_{qs} \\ i_{qr} \end{bmatrix} = \frac{1}{L_s L_r - L_m^2} \begin{bmatrix} l \end{bmatrix} \begin{bmatrix} \psi_{qs} \\ \psi_{qr} \end{bmatrix} \quad (6)$$

$$\begin{bmatrix} i_{ds} \\ i_{dr} \end{bmatrix} = \frac{1}{L_s L_r - L_m^2} \begin{bmatrix} l \end{bmatrix} \begin{bmatrix} \psi_{ds} \\ \psi_{dr} \end{bmatrix} \quad (7)$$

Where:

$$\begin{bmatrix} l \end{bmatrix} = \begin{bmatrix} L_r & -L_m \\ -L_m & L_s \end{bmatrix}$$

Now the state space model configuration of the DFIG in terms of stator and rotor flux linkages is given below in Eq. (8).

$$\frac{d}{dt} \begin{bmatrix} \psi_{qs} \\ \psi_{ds} \\ \psi_{qr} \\ \psi_{dr} \end{bmatrix} = \begin{bmatrix} A_s \end{bmatrix} \begin{bmatrix} \psi_{qs} \\ \psi_{ds} \\ \psi_{qr} \\ \psi_{dr} \end{bmatrix} + \begin{bmatrix} I_i \end{bmatrix} \begin{bmatrix} v_{qs} \\ v_{ds} \\ v_{qr} \\ v_{dr} \end{bmatrix} \quad (8)$$

Where $A_s = \begin{bmatrix} -\delta_1 & -\omega_e & \delta_2 & 0 \\ \omega_e & -\delta_1 & 0 & \delta_2 \\ \delta_3 & 0 & \delta_4 & (\omega_e - P\omega_r) \\ 0 & \delta_3 & (\omega_e - P\omega_r) & -\delta_4 \end{bmatrix}$

and $I_i = \begin{bmatrix} 1 & 0 & 0 & 0 \\ 0 & 1 & 0 & 0 \\ 0 & 0 & 1 & 0 \\ 0 & 0 & 0 & 1 \end{bmatrix}$

In the matrix A_s:

$$\delta_1 = \frac{R_s}{\sigma L_s},\ \delta_2 = \frac{R_s L_m}{\sigma L_s L_r},\ \delta_3 = \frac{R_r L_m}{\sigma L_s L_r},$$

$\delta_4 = \frac{R_r}{\sigma L_r}$ and $\sigma = \frac{L_s L_m - L_m^2}{L_s L_r}$ is defined as a leakage coefficient.

Again the state space model configuration of the DFIG in terms of rotor current and stator flux linkages is given below in Eq. (9).

$$\frac{d}{dt}\begin{bmatrix} \psi_{qs} \\ \psi_{ds} \\ i_{qr} \\ i_{dr} \end{bmatrix} = [B_s]\begin{bmatrix} \psi_{qs} \\ \psi_{ds} \\ i_{qr} \\ i_{dr} \end{bmatrix} + [C_s]\begin{bmatrix} v_{qs} \\ v_{ds} \\ v_{qr} \\ v_{dr} \end{bmatrix} \quad (9)$$

Where, $B_s = \begin{bmatrix} -\chi_1 & -\omega_e & 0 & \chi_2 \\ \omega_e & -\chi_1 & \chi_2 & 0 \\ 0 & -\chi_3 & \chi_4 & -\omega_{sl} \\ -\chi_3 & 0 & \omega_{sl} & -\chi_4 \end{bmatrix}$ and

$$C_s = \begin{bmatrix} 1 & 0 & 0 & 0 \\ 0 & 1 & 0 & 0 \\ 0 & 0 & \chi_5 & 0 \\ 0 & 0 & 0 & \chi_5 \end{bmatrix}$$

In the matrix B_s and C_s

$\chi_1 = \frac{R_s}{L_s},\ \chi_2 = \frac{R_s L_m}{L_s},\ \chi_3 = \frac{\omega_{sl} L_m}{\sigma L_r L_s},\ \chi_4 = \frac{R_r}{\sigma L_r}$ and

$\chi_5 = \frac{1}{\sigma L_r}$

4. Methodology

4.1. Rotor Side Control Scheme using PI controller

In rotor side, the main objective of the control system which are designed for rotor side converter to control the flow of power amid the stator and grid. For this purpose, control system needs the measurement of three phase stator voltage, rotor position, rotor current, and stator current. Basically, rotor side controller embraces two closed control loop which are shown in the Fig 2 [26, 27]. First one is inner control loop which is also known as rotor current control loop in which the real rotor current is compared with the reference value of current for generating the demanded rotor voltages. Second one is outer control loop which is also known as power control loop in which we are comparing the actual and reference power values for generating the demanded rotor current [23]. In this work, mathematical model is used in the place of outer loop control for calculating the rotor current references with the help of power references by using non-dynamic expressions. Basically here we are using voltage orientation control strategy so the stator voltage is aligned with quadrature axis of excitation reference frame. Along this one assumption has been made here that applied stator voltage is constant and the voltage drop on the stator resistance is insignificant so the voltage across the q-axis is equal to stator constant voltage and the voltage across the d-axis will be zero. In this work, the quadrature axis flux is controlled to be zero and direct axis flux is equal to value of stator flux. For decoupling the active and reactive all the expression is presented below:(d= d/dt throughout the paper) [27].

$$\begin{cases} d\psi_{qs} + \delta_1\psi_{qs} = v_{qs} + \delta_2\psi_{qr} - \omega_e\psi_{ds} \\ \sigma_{\psi qs} = v_{qs} + \delta_2\psi_{qr} - \omega_e\psi_{ds} \\ \psi_{ds}^* = \frac{1}{\omega_e}(v_{qs} + \delta_2\psi_{qr} - \sigma_{\psi qs}) \end{cases} \quad (10)$$

$$\begin{cases} d\psi_{ds} + \delta_1\psi_{ds} = v_{ds} + \omega_e\psi_{qs} + \delta_2\psi_{dr} \\ \sigma_{\psi ds} = v_{ds} + \omega_e\psi_{qs} + \delta_2\psi_{dr} \\ \psi_{qs}^* = \frac{1}{\omega_e}(\sigma_{\psi ds} - \delta_2\psi_{dr} - v_{ds}) \end{cases} \quad (11)$$

Substituting ψ_{qs}=0 in Eq. (3) and Eq. (4) results in Eq. (12)

$$\begin{cases} T_{em} = 1.5\psi_{ds} i_{qs} \\ i_{qs} = -\frac{L_m}{L_s} i_{qr} \end{cases} \quad (12)$$

From Eq. (10), we get

$$T_{em} = 1.5\psi_{ds}(-\frac{L_m}{L_S})i_{qr} \quad (13)$$

$$i_{qr} = 0.67\left(\frac{\sigma_{\omega r}.L_s}{\psi_{ds}L_m} - \frac{T_m L_s}{\psi_{ds}L_m}\right) \quad (14)$$

Now, the active power supplied by stator is given as:

$$P_s = 1.5(v_{qs}i_{qs} + v_{ds}i_{ds}) \quad (15)$$

Putting v_{ds}=0 and the value of i_{qs}, we get

$$P_s = -1.5\frac{L_m}{L_s} v_{qs} i_{qr} \quad (16)$$

Putting the value of v_{qs} in Eq.(16)

$$P_s = -1.5\left(R_s i_{qs} + \omega_e\psi_{ds} + d\psi_{qs}\right)\frac{L_m}{L_s} i_{qr} \quad (17)$$

Now Put the value of i_{qr} from Eq. (6) in Eq.(17) and neglect the resistance of stator by keeping the stator flux constant:

$$P_s = -1.5\omega_e\psi_{ds}\frac{L_m}{L_s}\left[\frac{-L_m}{\sigma L_s L_r}\psi_{qs}+\frac{1}{\sigma L_r}\psi_{qr}\right] \quad (18)$$

Differentiating Eq. (18) w. r. t. time provides:

$$dP_s = -1.5\frac{\omega_e}{\sigma L_s}\frac{L_m}{L_r}\psi_{ds}\left[v_{qr}-R_r i_{qr}+\left(\omega_e-\omega_r\right)\sigma L_r i_{dr}\right] \quad (19)$$

Now the reactive power supplied by stator is given as:

$$Q_s = 1.5(v_{qs}i_{ds}-v_{ds}i_{qs}) \quad (20)$$

Putting the value of v_{ds} and v_{qs} in Eq. (20)

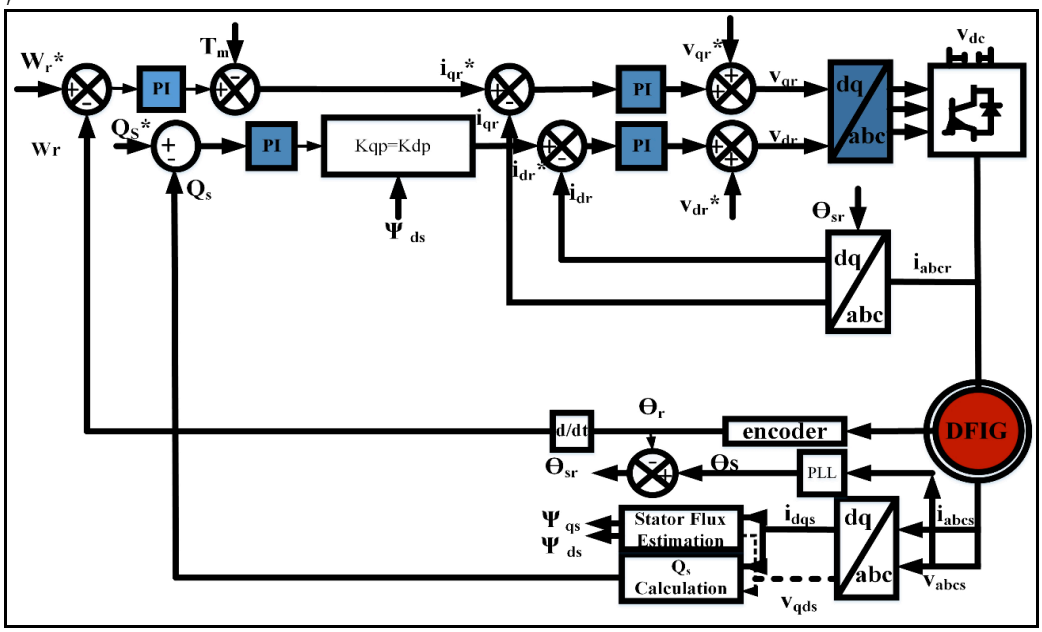

Fig. 2. Schematic representation of simulation block diagram of Rotor Side Control (RSC) strategy

$$Q_s = 1.5v_{qs}i_{ds} \quad (20.1)$$

$$Q_s = 1.5(R_s i_{qs}+\omega_e\psi_{ds}+s\psi_{qs})i_{ds} \quad (21)$$

Putting the value of i_{ds} from the Eq.(7) in Eq.(21) and neglect the resistance of stator by keeping the stator flux constant:

$$Q_s = 1.5(\psi_{ds}^2-\frac{L_m}{L_r}\psi_{ds}\psi_{dr})\frac{\omega_e}{\sigma L_s} \quad (22)$$

Differentiating Eq. (22) w. r. t. time provides:

$$dQ_s = -1.5\frac{\omega_e}{\sigma L_s}\frac{L_m}{L_r}\psi_{ds}d\psi_{dr} \quad (23)$$

The rotor side d and q axis voltages expression from the Eq. (2) and Eq. (5) is given below as:

$$v_{qr} = R_r i_{qr}+\omega_{sl}\left(\frac{L_m}{L_s}\psi_{ds}+\sigma L_r i_{dr}\right)+\sigma L_r di_{qr} \quad (24)$$

$$v_{dr} = R_r i_{dr}-\omega_{sl}\sigma L_r i_{qr}+\sigma L_r di_{dr} \quad (25)$$

where $\omega_{sl} = (\omega_e-\omega_r)$ is defined as a slip speed.

Then the q- axis and the d-axis reference voltage of the rotor side are given as:

$$v_{qr}^* = \sigma_{qr}+\omega_{sl}(\frac{L_m}{L_s}\psi_{ds}+\sigma L_r i_{dr}) \quad (26)$$

$$v_{dr}^* = \sigma_{dr}-\omega_{sl}(\sigma L_r i_{qr}) \quad (27)$$

The control arrangement of rotor side converter (RSC) is displayed below in Fig. 2.

4.2. Rotor Side Control Scheme using ANN controller

For the rotor side control by using ANN controller, we used Levenberg-Marquardt algorithm for training purpose. The purpose of MATLAB Toolbox is to open the window of Data Manager of Neural Network and with the help of this, operator import, build and then export neural networks and data are produced [28]. Following Table 1 explained all Network characters of my proposed research work in rotor side control [28, 29].

Table 1. Network Characters of ANN Training Window in rotor side

S.No.	Network Types	Network Characters
1.	Inputs of the Network	Direct axis and quadrature axis rotor current
2.	The output of the Network	Real and reactive power of the stator
3.	Training Function	TRAINLM
4.	Network Configuration	Feed-Forward Backpropagation
5.	Adjustment learning function	LEARNGDM
6.	Function of Performance	Mean Square Error (MSE)
7.	Number of neurons in Hidden Layers	8

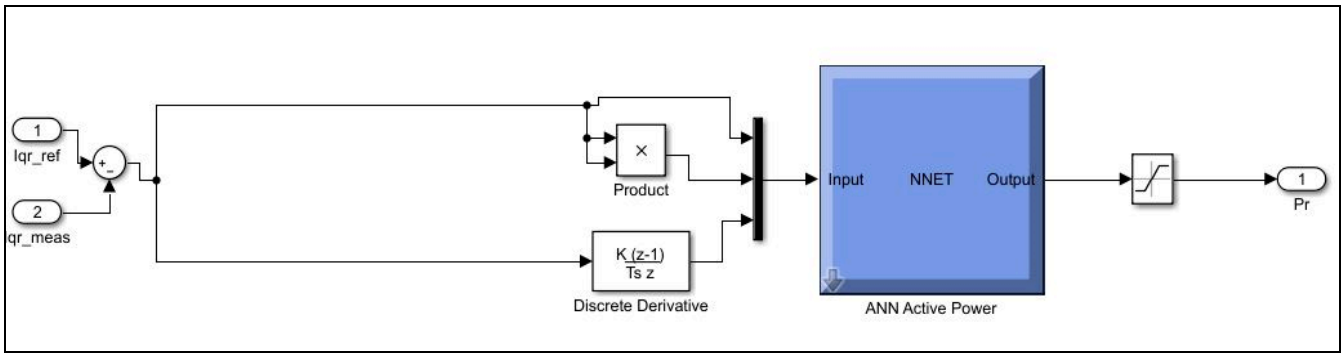

Fig. 3. Schematic representation of the ANN controller (Simulink model) for stator active power control in rotor side

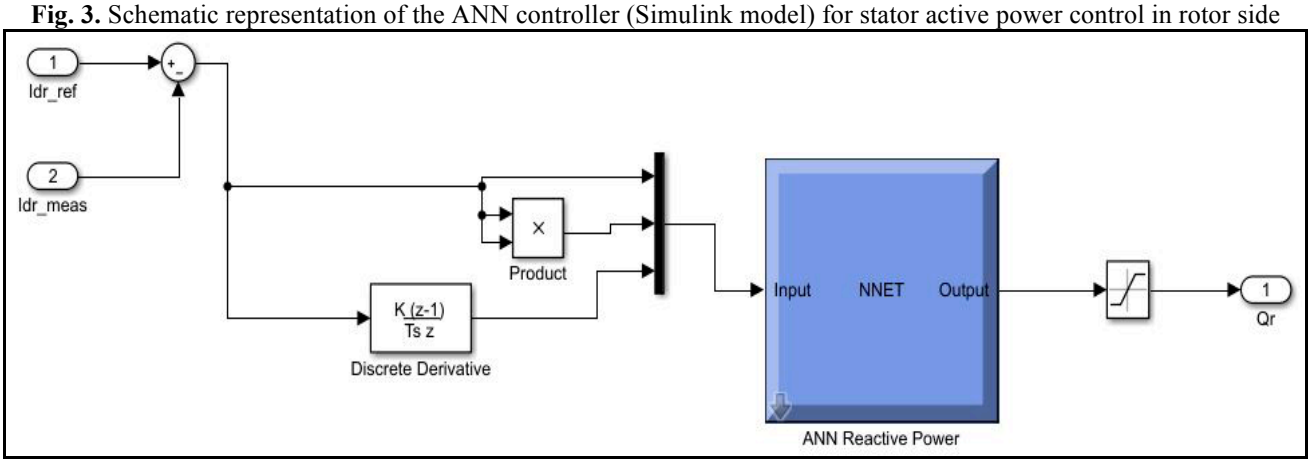

Fig. 4. Schematic representation of the ANN controller (Simulink model) for stator reactive power control in rotor side

In this simulation, for active power control, we are comparing the reference and actual values of q-axis rotor current. The comparative value is fed to ANN controller in the form of multi-input which is clearly shown in the Fig.3. The number of neurons which are used in hidden layer is 8. The input is fed to ANN controller by product block and for previous sample values, we are using discrete derivative. So, the configuration 3-8-1 is used for generating the desired value of output in rotor side.

Same as the active power control, we are using ANN controller for stator reactive power control. Here we are comparing the reference and actual values of d-axis rotor current for generating the desired reactive power as shown in the Fig.4. All other procedure is same like as active power control in rotor side control.

4.3. Grid Side Control Scheme using PI controller

The purpose of control system which are designed for grid side converter to maintain the active power transferred between the rotor circuit and grid by controlling the DC bus voltage [26]. The reactive power amid the RSC and GSC is decoupled due to exciting of the DC bus. So reactive power

of the grid side can be controlled independently. Similar to rotor control system, the vector controlled scheme which are

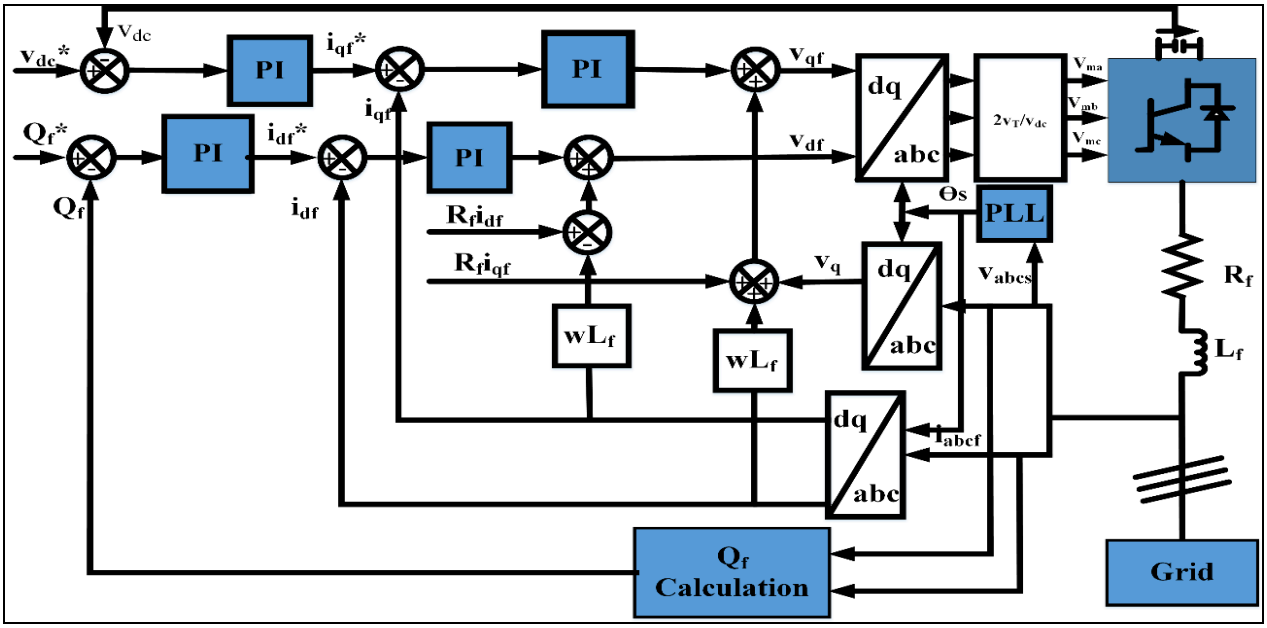

Fig. 5. Schematic representation of simulation of Grid Side Converter control strategy

used in grid side converter needs the instant values of the DC link voltage, three phase converter currents and three phase stator voltage. The converter which are used in grid side is current regulated converter so the direct axis converter current is used to control the dc bus voltage and quadrature axis current are used to control the reactive power. Grid side converter contains two closed loop control similar to rotor side converter. First, one is outer loop control which controls the DC bus voltage and maintains at a constant level irrespective of path and magnitude of the rotor power with the help of producing demanded d-q converter currents and second one is internal loop controls the grid side reactive power at zero level for unity power factor operation [26, 27, 36, 37].

In the DC bus, the voltage expression is given as:

$$C_{dc}dv_{dc} = 0.75(\mathrm{m}_{df}\, i_{df} + m_{qf}i_{qf} + m_{dr}i_{dr} + m_{qr}i_{qr}) \quad (28)$$

Where

C_{dc} = capacitance of the DC bus

m_{qf} = Modulation index of GSC in q-axis

m_{df} = Modulation index of GSC in d-axis

m_{dr} = Modulation index of RSC in d-axis

m_{qr} = Modulation index of RSC in q-axis

d =first derivative (d/dt) throughout the paper

Equation (28) can be remodified which is presented in Eq. (29)

$$\sigma_{dc} = 0.75(m_{df}i_{df} + m_{qf}i_{qf} + m_{dr}i_{dr} + m_{qr}i_{qr}) = C_{dc}dv_{dc} \quad (29)$$

From Eq. (28), q-axis grid current is given below:

$$i_{qf}^{*} = 1.33\frac{1}{m_{qf}}\left(\sigma_{dc} - 0.75\left(m_{qr}i_{qr} + m_{dr}i_{dr}\right)\right) - \frac{m_{df}}{m_{qf}}i_{df} \quad (30)$$

displayed below in Fig. 5 [26, 27] .

By using KVL across the RL filter, which gives the expressions of q and d-axis voltages of the grid side in Eq. (31) and Eq. (32)

$$v_{qf} = R_f i_{qf} + L_f di_{qf} + \omega_e L_f i_{df} + \frac{v_{qs}}{N_T} = 0.5m_{qf}v_{dc} \quad (31)$$

$$v_{df} = R_f i_{df} + L_f di_{df} - \omega_e L_f i_{qf} = 0.5m_{df}v_{dc} \quad (32)$$

The reactive power delivered by grid side converter using the condition that v_{ds}=0 and $v_{qs} = v_s$ is given as:

$$Q_f = \frac{1.5}{N_T}i_{df}v_s \quad (33)$$

In Eq. (33), N_T is illustrated as the turns ratio of the transformer connected between stator and GSC.

$$dQ_f = 1.5di_{df}\frac{v_s}{N_T} \quad (34)$$

After substituting the Eq. (32) in Eq. (34)

$$dQ_f = 1.5\frac{v_s}{N_T L_f}\left(v_{df} - R_f i_{df} + \omega_e L_f i_{qf}\right) \quad (35)$$

$$\gamma_1 dQ_f = (v_{df} - R_f v_{df} + \omega_e L_f i_{qf}) = \sigma_{Qf} \quad (36)$$

In Eq. (36), $\gamma_1 = \dfrac{0.67L_f N_T}{v_s}$

From Eq. (36), d-axis grid current is given below:

$$i_{df}^{*} = \frac{1}{R_f}(v_{df} + \omega_e L_f i_{qf} - \sigma_{Qf}) \quad (37)$$

From the inner current regulation of the grid side converter;

$$R_f i_{qf} + L_f di_{qf} = K_{qf}(i_{qf}^{*} - i_{qf}) = \sigma_{qf} \quad (38)$$

$$R_f i_{df} + L_f di_{df} = K_{qf}(i_{df}^{*} - i_{df}) = \sigma_{df} \quad (39)$$

The Grid Side Converter (GSC) control arrangement is

Table.2. Network Characters of ANN Training Window in grid side control

S.No.	Network Types	Network Characters
1.	Inputs of the Network	Direct axis and quadrature axis converter current
2.	The output of the Network	Grid reactive power, Dc bus voltage
3.	Training Function	TRAINLM
4.	Network Configuration	Feed-Forward Backpropagation
5.	Adjustment learning function	LEARNGDM
6.	Function of Performance	Mean Square Error (MSE)
7.	Number of neurons in Hidden Layers	8

4.4. Grid Side Control Scheme using ANN controller

For grid side control, again we used Levenberg Marquardt algorithm for training purpose. Following Table 2 explained all Network characters of my proposed research work in grid side control [28, 29, 30].

In this simulation sub-model, we are controlling the voltage across the DC bus and maintain at a constant level for superior performance. Again 3-8-1 configuration is used so 3 inputs are provided to hidden layer whereas in hidden layer contains 8 neurons and sigmoid functions, as well as output function, contains the linear function which is shown in the Fig. 6.

Same as the DC bus control, we are using ANN controller for grid reactive power control. Here we are comparing the reference and actual values of q-axis converter current for generating the desired reactive power as shown in the Fig.7 [31,32, 33]. All other procedure is same like as DC bus voltage control in grid side control [34, 35, 36, 37].

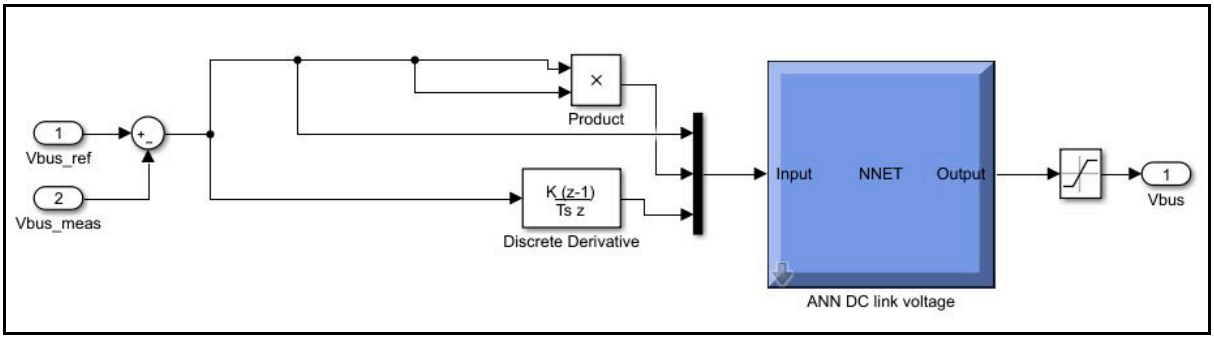

Fig. 6. Schematic representation of the ANN controller (Simulink model) for DC bus control in grid side

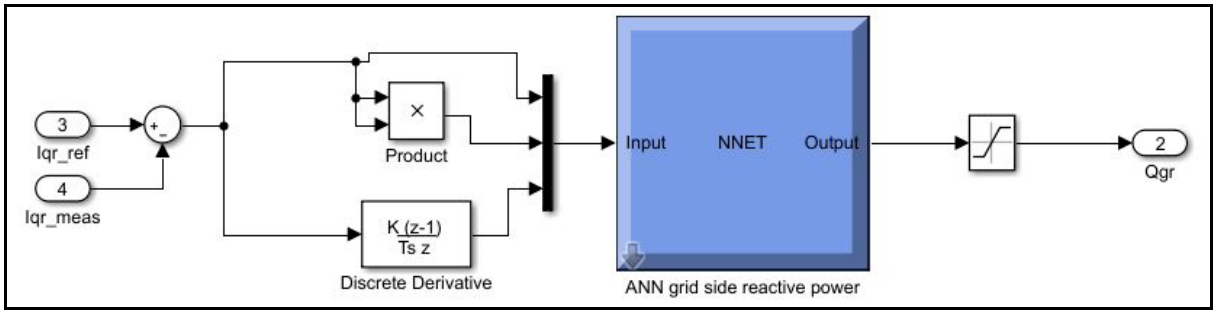

Fig. 7. Schematic representation of the ANN controller (Simulink model) for reactive power control in grid side

5. Simulation Results and Discussion

In this segment, the simulation responses are carried out with 2 MW DFIG for 2 MW SHPP coupled with constant voltage and constant frequency grid using MATLAB/SIMULINK software. The overall responses in PI and ANN controller are summarised in tabulated in Table 3 and Table 4. The both control techniques are PI and ANN are simulated and compared regarding stator real power, reactive power, stator current, rotor current rotor speed in rotor side control and DC link voltage and reactive power in the grid side control.

5.1. Tracking of reference rotor speed

The motive of this section to presents the comparative analysis of simulated responses of both controller (PI and ANN) of the control dynamic of DFIG in three different modes of speed operation with high stability and linear transition response using vector control method. In the responses, the time simulation is three seconds and each second represents one mode as shown in figures. So the time duration from 0 to 1sec is illustrated as sub-synchronous mode, 1 to 2 sec is presented as synchronous mode and 2 to 3 sec is illustrated as super synchronous mode. At starting the reference speed is set at 125.6 rad/sec that signifies sub-synchronous mode, then at t=1sec the rotor speed is changed to 157 rad/sec to align the machine synchronous speed and after this at t=2sec again rotor speed increases and attained the super synchronous speed i.e.188.4 rad/sec which is clearly shown in the Fig.8 and Fig.9. Figure 8 represents the rotor speed due to PI controller and Fig. 9 presents the rotor speed due to ANN controller. It is clearly shown in the figures that ANN controller significantly improves the speed response as compare to traditional PI controller by completely eliminating the speed overshoot in different speed modes. This modification improves the machine performance as well as provides the smooth and sluggish free outputs.

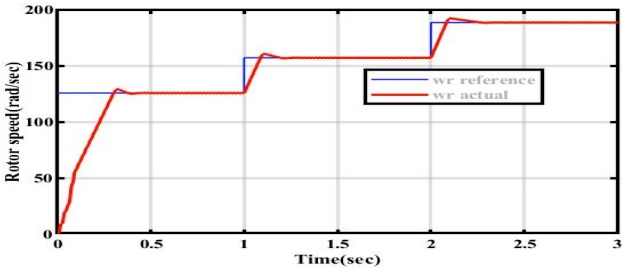

Fig. 8. Rotor speed of the DFIG (PI controller)

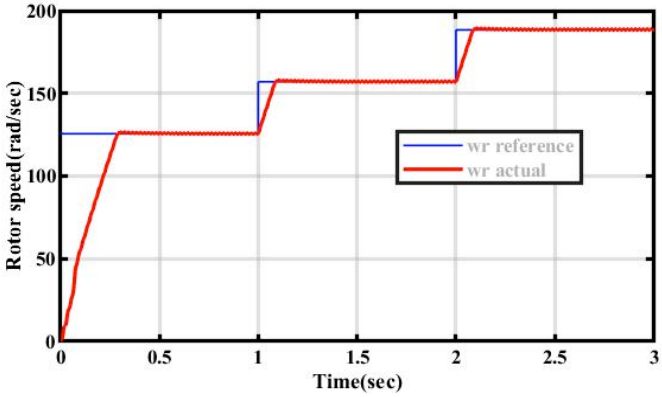

Fig. 9. Rotor speed of the DFIG (ANN controller)

5.2. DFIG Real and Reactive Power Flow

In all three modes, the state of stator active and stator reactive power flow are presented in Fig.10, Fig.11, Fig.12 and Fig. 13. The sign of active power illustrates the direction of power like positive power specifies that the power goes into the DFIG and negative power designates that power goes towards the grid. However, the stator active power increasing with increasing speed from sub-synchronous mode to super synchronous mode whereas the reactive power will be zero throughout all the modes. In the below shown Fig.10 represents the stator active power with PI controller. In sub-synchronous mode, the stator supplied 1.3 MW to the grid, in synchronous mode, flow of power increases from 1.3 MW to 1.6 MW and in super-synchronous mode again active power increases from 1.6 MW to 1.7 MW. But due to more nonlinearity of DFIG, PI controller is unable to diminishing the overshoot which is clearly shown in the Fig.10. For significantly improvising the system response ANN controller is implemented which rectifying the overshoot in stator active power which is shown in the Fig.11 and it is lucidly visible that subsequently preliminary transient state disappears, stator active power is highly smooth during the one speed mode to another speed mode. Stator active power with ANN controller generate more power as compare to PI controller like in sub-synchronous mode stator generate 1.48 MW and it increased to 1.67 MW when speed changes from 125.6 rad/sec to 157 rad/sec and when rotor will attain the super-synchronous speed (188.4rad/sec), the stator power will increase to 1.86 MW. The stator active is set to be zero throughout all the speeds but in the case of PI controller, the reactive power affected by undershoot which is clearly shown in Fig. 12 when the rotor changes speed from one mode to another mode. With the ANN controller, stator supplies zero reactive power without any undershoot which is shown in the Fig.13.

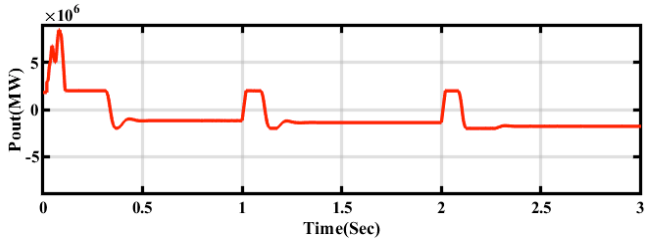

Fig. 10. DFIG stator active power (PI controller)

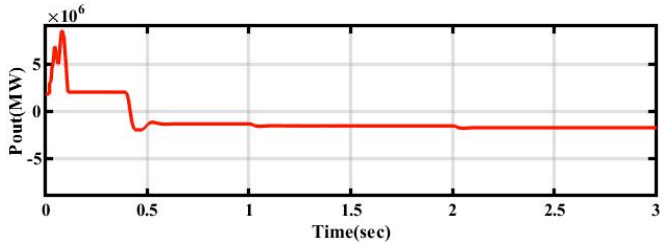

Fig. 11. DFIG stator active power (ANN controller)

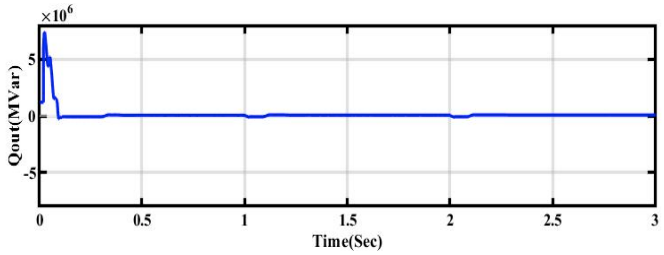

Fig. 12. DFIG stator reactive power (PI controller)

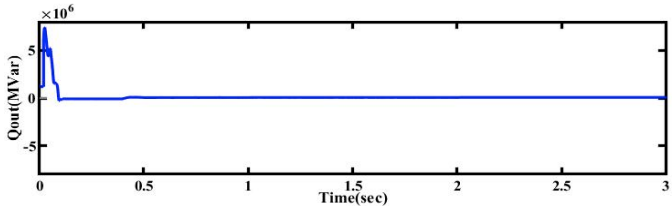

Fig. 13. DFIG stator reactive power (ANN controller)

5.3. Three-Phase Voltage and Current of the System

Three phase stator voltage, stator current, and rotor current are shown in the Fig.14, Fig.15, Fig.16, Fig.19 and Fig.20. During the rotor speed shift from less than synchronous speed to greater than synchronous speed, the stator voltage, and stator current will be constant and stable. But the rotor current will be change according to change in speed which is clearly shown in the Fig. 19 and Fig.20. it can be seen that in less than synchronous speed, the phase sequence of the rotor current will be (abc) and the value of slip will be positive. Whereas when rotor reaches the super-synchronous mode, the phase sequence which has been in rotor current is (acb) and value of slip will be negative. In synchronous mode, the rotor circuit turns to DC circuit hence rotor current follows constant dc waveform. The magnitude of the rotor current will be always less than stator current because, in rotor current, the value of slip also included. Figure 17 and Fig. 18 describe the FFT analysis of the stator current by PI and ANN controller. The value of THD of stator current due to PI controller is 5.40% and with the help of ANN controller, the THD of stator is significantly improved from 5.40% to 3.88%. The rotor current with PI controller has some peak overshoot while changing the mode of speed. To reduce this unwanted overshoot, ANN controller has been successfully implemented and controller diminishes overshoot of rotor current as shown in Fig.19 and Fig.20.

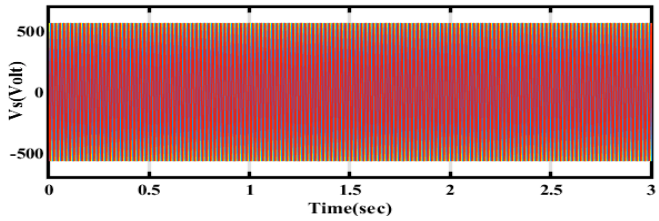

Fig. 14. Stator voltage

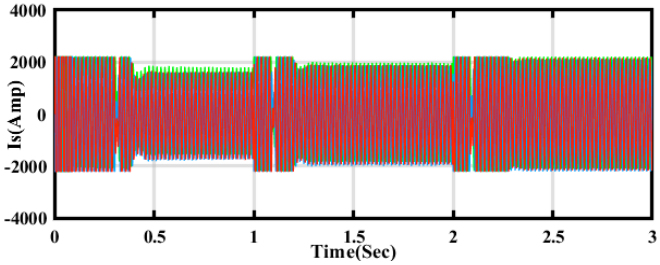

Fig. 15. Stator current (PI controller)

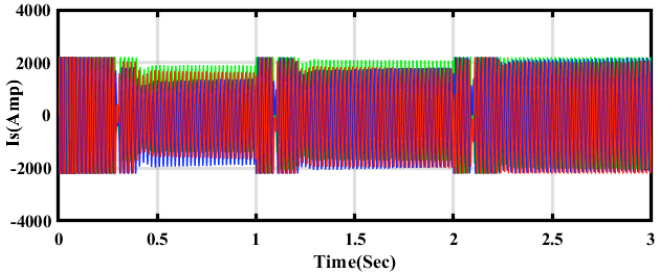

Fig.16. Stator current (ANN controller)

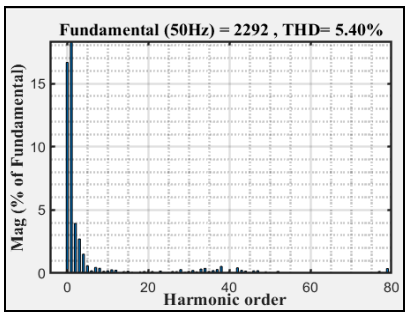

Fig. 17. FFT analysis in stator current due to PI controller

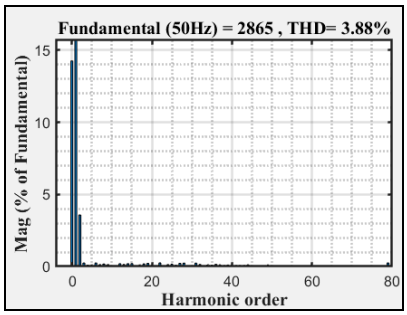

Fig. 18. FFT analysis in stator current due to ANN controller

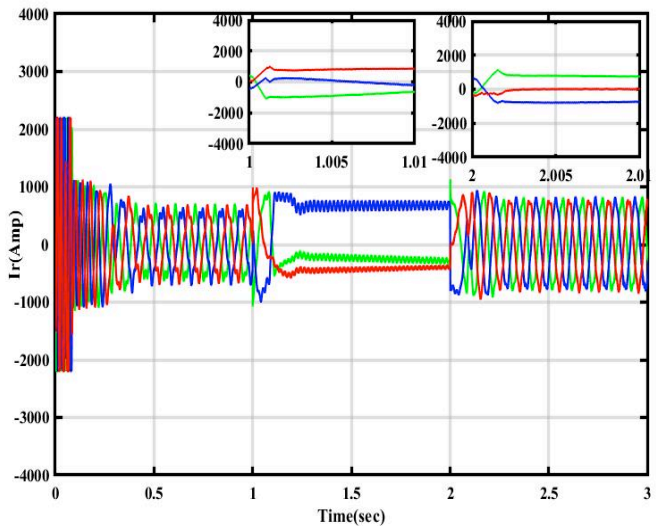

Fig. 19. Rotor current (ANN Controller)

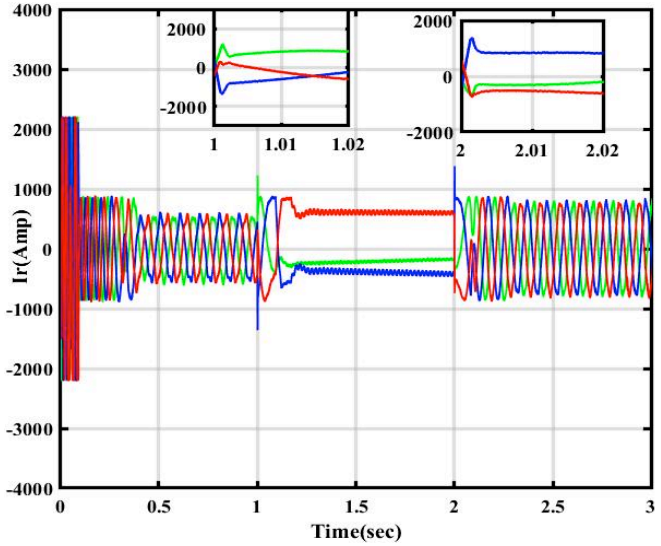

Fig. 20. Rotor current (PI Controller)

5.4. DC Link voltage and Grid reactive power:

The reactive power of the rotor side converter and the reactive power of the grid side converter are decoupled because of existence of DC bus so the presence of DC bus is very much essential. The voltage across the DC-link is to keep at a constant level for controlling the balance between the charging and discharging power of the capacitor. As shown in the Fig.23 and Fig.24, the DC bus voltage is to keep constant at 1150 volt but due nonlinearity of DFIG the DC bus voltage influenced by more undershoot so it starts from zero and attains the constant 1150-volt value but for more satisfactory operation and for diminishing this undershoot, ANN controller has been used as shown in the Fig. 24 and this controller undoubtedly reduced more undershoot and from simulation result it is visible that dc bus voltage in the case of ANN controller starts from 1000-volts and within very minor attains the 1150- volt value and make the system more apposite for real time application. One thing is very much clear that in DC bus voltage simulation responses, there is no any ripple due to this system become more apposite. For unity power factor operation, the grid side reactive power must be at zero level. The simulated outcomes of grid reactive power because of PI and ANN controller are shown in the Fig. 21 and Fig. 22. It is clearly visible that reactive power is set at zero level as well as for reducing the overshoot and undershoot in grid reactive power, ANN controller is implemented which is shown in the Fig.22.

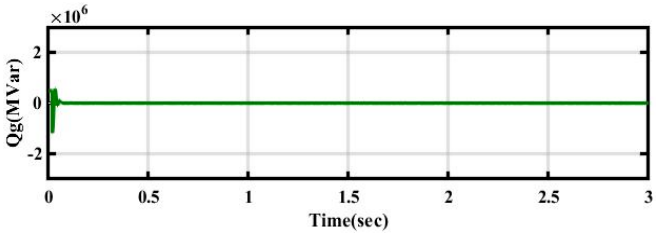

Fig. 21. Grid reactive Power (PI controller)

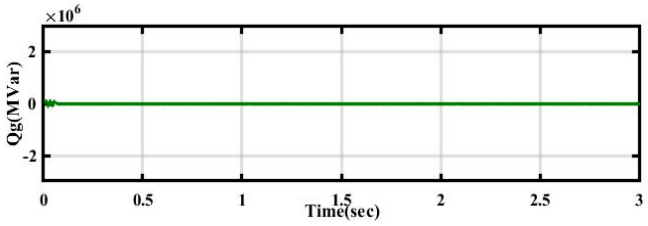

Fig. 22. Grid reactive power (ANN controller)

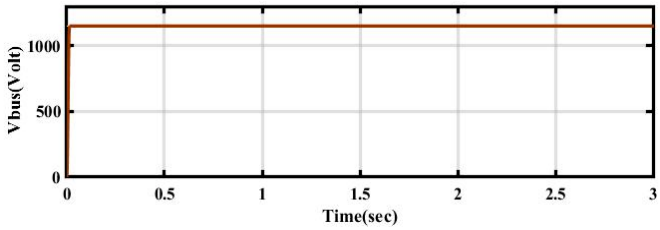

Fig. 23. DC bus voltage (PI controller)

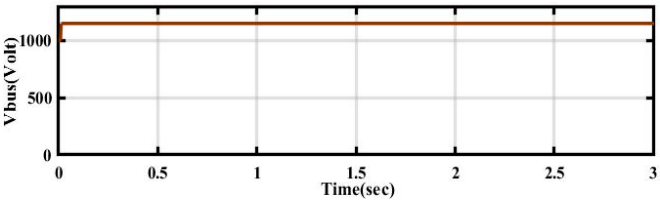

Fig. 24. DC bus voltage (ANN controller)

Moreover, these applied two control strategies lead to more noticeable differences in all simulated outcomes. To validate the effectiveness of presented two control strategies, we have reported in the Table 5. The performance analysis of PI and ANN controller is shown graphically in Fig. 25, Fig. 26 and Fig. 27.

Table 3. Description of the performance of 2 MW SHPP linked with 2 MW DFIG at different modes of speed operation with PI controller

Rotor speed, wr(rad/sec)	Stator current frequency, I_{sf} (Hz)	Rotor current frequency, I_{rf} (Hz)	Stator active power, Pout(MW)	Stator reactive power, Qout (MVar)	Stator voltage (Volt)	DC bus voltage, Vbus (Volt)	Grid reactive power, Qgr(MVar)
125.6	50	10	-1.3	00	690	1150	00
157	50	00	-1.6	00	690	1150	00
188.4	50	-10	-1.7	00	690	1150	00

Table 4. Description of the performance of 2 MW SHPP linked with 2 MW DFIG at different modes of speed operation with ANN controller

Rotor speed, wr(rad/sec)	Stator current frequency, I_{sf} (Hz)	Rotor current frequency, I_{rf} (Hz)	Stator active power, Pout(MW)	Stator reactive power, Qout (MVar)	Stator voltage (Volt)	DC bus Voltage, Vbus (Volt)	Grid reactive power, Qgr(MVar)
125.6	50	10	-1.48	00	690	1150	00
157	50	00	-1.67	00	690	1150	00
188.4	50	-10	-1.86	00	690	1150	00

Table 5. Performance Analysis of ANN and PI controller in the terms of Rotor speed in all speed modes

Modes	Sub-synchronous mode		Synchronous mode		Super-synchronous mode	
Controllers / Parameters	PI	ANN	PI	ANN	PI	ANN
Overshoot(%)	2.22	0.397	2.03	0.445	1.96	0.371
Settling time (Sec)	0.4443	0.3213	1.228	1.101	2.31	2.10
Rise time (Sec)	0.6459	0.4136	1.366	1.212	2.429	2.187

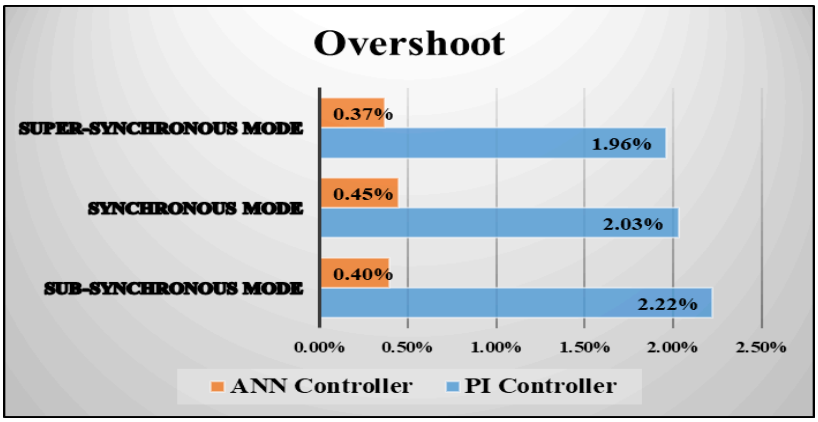

Fig. 25. Graphical representation of comparison of overshoot in rotor speed.

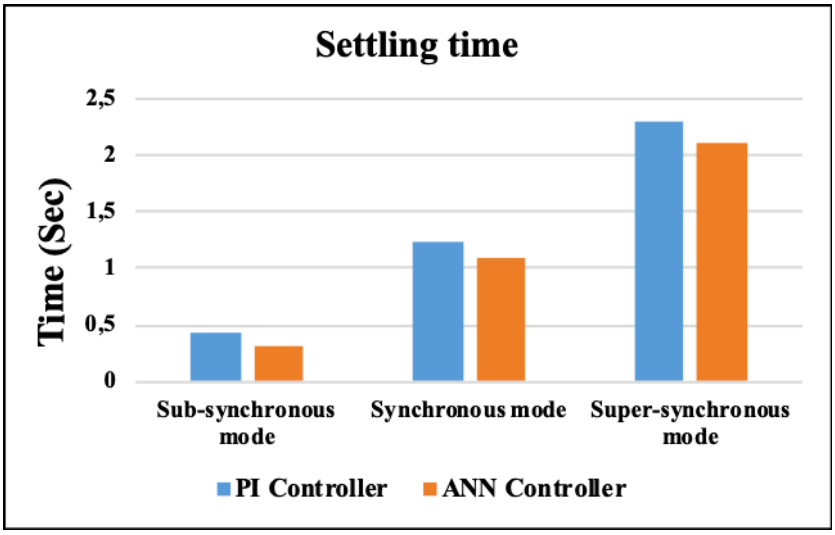

Fig. 26. Pictorial representation of comparison of settling time in rotor speed.

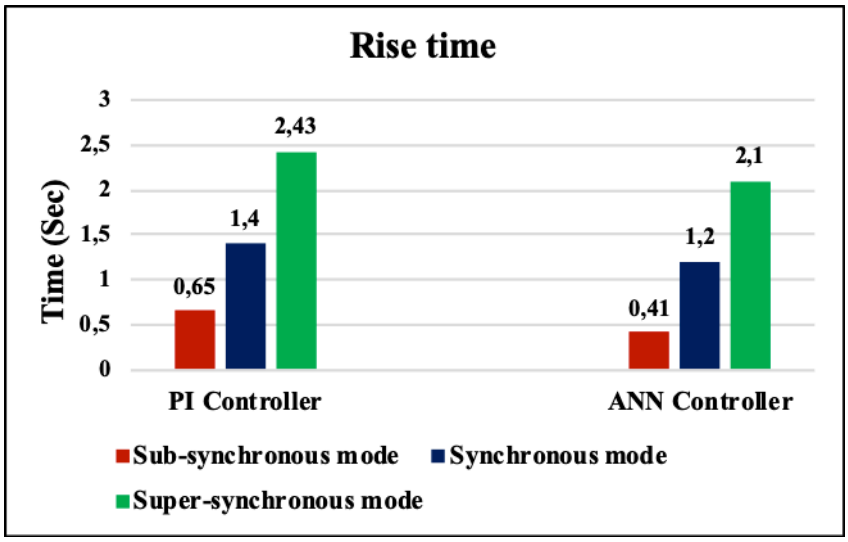

Fig. 27. Illustrative representation of comparison of rise time in rotor speed.

6. Conclusion

The foremost objective of this proposed work is to present performance comparative of working of two different control strategies applied on Grid connected DFIG based small hydropower power plant. Two important objectives are set for this work. First one is to generate desired stator power to meet the requirement of the customer. As generally small hydro plant fulfills the demand of peak value. Depending upon the which are applied in the rotor side for controlling active and reactive in the entire range of turbine speed. Reactive power in the rotor side is to keep at zero level so we can generate more active power for feeding to the grid as well as for better power factor operation. Now the second objective is to set reactive power at zero level for zero power factor angle operation in the grid side and maintain the dc link voltage at a constant level for maintaining the optimum operation of rotor side. The first control strategies are PI controller using voltage orientation control (VOC) scheme and the second one is a new simple and more efficient Artificial Neural Network controller which are using computational intelligence. The main contribution of this research paper to represent the proper control of real and reactive power in rotor side and regulates the reactive power and voltage across the dc bus in grid side by using both PI and ANN control scheme. But due to the nonlinearity of the DFIG model, PI control scheme is unable for giving smooth and sluggish-free results. For improving the transient behaviour in large extent as well as improving the typical second order parameters such as rise time, peak time, settling time, overshoot and undershoot, ANN control scheme has been successfully implemented. All the presented simulation results undoubtedly confirm that proposed novel ANN controller schemes is successful in providing a transient free response in rotor side and grid side along with this scheme also provides more active power in different speed mode as compare existing control scheme. For real-time implementation, we can use real-time simulator lab (RT-LAB) or digital signal processor (DSP). The same simulation model which has been presented in the control scheme can be

used in RT-LAB or DSP and the results acquired from RT-LAB will be similar to all presented results.

Appendix

Table 6. The Parameters for 2 MW DFIG that have been used for designing the simulation model:

Parameters	Values	Units
Rated Output Power	2	MW
Rated frequency	50	Hz
Stator Voltage	690	Volt
Stator/Rotor turns ratio	0.33	-
Poles	4	-
Rotor Resistance	2.9	mΩ
Stator Resistance	2.6	mΩ
Rotor Inductance	2.58	mH
Stator Inductance	2.58	mH
Mutual Inductance	2.5	mH
Turbine rotor speed	157	rad/sec
Inertia Constant	3.82	Sec

Acknowledgements

This research work was endorsed by National Institute of Technology, Jamshedpur, India. The first and second author is highly obliged to associate professor Dr. Madhu Singh (NIT, Jamshedpur) for endless guidance to complete this research work.

References

[1] Lari Shanlang Tiewsoh, Jakub Jirásek, and Martin Sivek, “Electricity Generation in India: Present State, Future Outlook and Policy Implications”, Energies, vol. 12 no.7, pp. 1-14, 2019.

[2] S. Camel, F. Teng, A. Michiorri, G. Kariniotakis, and L. Badesa, “Scenario generation of aggregated Wind, Photovoltaics and small Hydro production for power systems applications”, Applied Energy, vol. 242, pp. 1396-1404, 2019.

[3] Srikanth, R. “India's sustainable development goals – Glide path for India's power sector”, Energy Policy, vol. 123, pp. 325-336, 2018.

[4] Md. Mustafa Kamal, “Scenario of Small Hydro Power Projects in India and Its Environmental Aspect”, International Research Journal of Engineering and Technology (IRJET), vol. 04, no. 10, pp. 228-234, 2017.

[5] Vineet Kumar Singh, S. K. Singal, “Operation of hydro power plants-a review”, Renewable and Sustainable Energy Reviews, vol. 69, pp. 610-619, 2017.

[6] C. P. Jawahar, Prawin Angel Michael, “A review on turbines for micro hydro power plant”, Renewable and Sustainable Energy Reviews, vol. 72, pp. 882-887, 2017.

[7] Mishra M K, Khare N, Agrawal A B, “Small Hydro Power in India: Current Status and Future Perspectives”, *Renewable and Sustainable Energy Reviews* 51(2015), 101-115, 2015.

[8] The government of India, “The National Electricity Plan”, Ministry of New and Renewable Energy, Jan 2017.

[9] Maximiliano Ferrari, “GSC Control Strategy for Harmonic Voltage Elimination of Grid- Connected DFIG Wind Turbine,” 2014 *International Conference on Renewable Energy Research and Application*s (*ICRERA*), Milwakuee, USA, pp. 185-191, 2014.

[10] L. Morel, H. Godfroid, A. Mirzaian, and J. M. Kauffman, “Double-fed induction machine: converter optimisation and field oriented control without position sensor,” *IEE Proceedings on Electric Power Applications*, vol.145, pp. 360-368, 1998.

[11] H. Ko, G. Yoon, N. Kyung, and W. Hong, “Modeling and control of DFIG-based variable-speed wind turbine,” *Electric Power System Research*, vol.78, no. 11, pp.1841-1849, 2008.

[12] A. R. Ghumman et al, Runoff forecasting by the artificial network and conventional model, *Alexandria Eng. J.* vol. 50 no.4, pp.345-350, 2011.

[13] S. Haykin, *Neural Networks,* 2nd Edition, Prentice Hall, 1999, ISBN 0-13-273350.

[14] L. M. Fernandez, C. A. Garcia, F. Jurado, and J. R. Saenz, "Aggregation of doubly fed induction generators wind turbines under different incoming wind speeds," *IEEE Russia Power Tech*, St. Petersburg, pp. 1-6, 2005.

[15] X. Yao, S. Liu, X. Wang, C. Guo, Z. Xing, and H. Jiang, “Doubly-fed Induction generator control for variable-speed wind power generation system,” in Proceedings of the *IEEE International Conference on Mechatronics and Automation* (*ICMA* ’09), pp. 855–859, August 2009.

[16] I. Boldea. Variable speed generators. CRC, 2005.

[17] U. K. Madawala, T. Geyer, J. B. Bradshaw, and D. M. Vilathgamuwa, "Modeling and Analysis of a Novel Variable-Speed Cage Induction Generator," in *IEEE Transactions on Industrial Electronics*, vol. 59, no. 2, pp. 1020-1028, Feb. 2012.

[18] S. Auddy, R. K. Varma and M. Dang, "Field Validation of a Doubly Fed Induction Generator (DFIG) Model," *IEEE Canada Electrical Power Conference*, Montreal, Que., pp. 484-489, 2007.

[19] Y. Lei, A. Mullane, G. Lightbody, and R. Yacamini, “Modeling of the wind turbine with a doubly fed induction generator for grid integration studies,” *IEEE Transactions on Energy Conversion*, vol. 21, no. 1, pp. 257–264, 2006.

[20] J. G. Slootweg, H. Polinder, and W. L. Kling, "Dynamic modeling of a wind turbine with doubly fed induction generator," in *Proceedings of the 2001 IEEE Power Engineering Society Summer Meeting,* vol. 1, pp. 644–649, July 2001.

[21] I. Boldea and S. Nasar. The induction machine handbook. CRC, 2001.

[22] M.S. Hamad, K.H. Ahmed, "A Multifunctional Current Source Inverter Control for Wind Turbine Grid Interfacing", 2015 *International Conference on Renewable Energy Research and Applications* (*ICRERA*), Palermo, Italy, pp. 1328-1331, 2015.

[23] Zhao Y, Zou X, Huang D, Liu X, Cao F, Kang Y, "Research on Excitation Control of Flexible Power Conditioner Doubly Fed Induction Machine", IEEE, Power Electronics Specialists Conference, PESC 2007, pp. 92-97, 17-21 June 2007.

[24] Janaka B. Ekanayake, Lee Holdsworth, Xueguang Wu and Nicholas Jenkins "Dynamic Modeling of Doubly-fed Induction Generator Wind Turbines", IEEE Transactions on Power Systems, Vol.18, No.2, pp.803-809, May 2003.

[25] P. Vas. Vector Control of AC machines. Clarendon Press Oxford, 1990.

[26] Sanjeev Kumar Gagrai, Sundram Mishra, Madhu Singh "Performance Analysis of Grid Integrated Doubly Fed Induction Generator for a Small Hydro Power Plant", *International Journal of Renewable Energy Research*, Vol.8, No. 4, pp.2311-2323, 2018.

[27] S. N. Sivanandam, Sumathi, and Deepa, "Introduction to neural networks using MATLAB 6.0," Tata McGraw-Hill Education, 2006.

[28] X. Yu, C. Ye, and L. Xiang, "Application of artificial neural network in the diagnostic system of osteoporosis", *Neurocomputing*, vol. 214, pp.376-381, 2016.

[29] Jagannath Ch yadav. B, KVR Swathi, "Simulation and Control of a Doubly Fed Induction Generator (DFIG) Using Artificial Neural Networks" *International Journal of Engineering Research and Applications (IJERA),* Vol.2, No.5, pp.102-106, 2012.

[30] S. Mishra, S. K. Gagrai and M. Singh, "An ANN Based Simulation and Control of Grid Integrated DFIG for 2 MW Small Hydro Power Plant," *6th International Conference on Signal Processing and Integrated Networks (SPIN*), Noida, India, pp. 540-546, 2019.

[31] Sanjeev Kumar Gagrai, Sundram Mishra, and Madhu Singh, "Dynamic Modelling and Simulation of Grid Coupled DFIG Designed for 2 MW SHPP Using ANN Scheme", Journal of Engineering and Applied Sciences, vol.14, no.11 pp. 3813-3831, 2019.

[32] Azzouz Said, Messlati Sabir, "Control of Active and Reactive Power of DFIG by Artificial Neural Networks", Journal of Engineering and Applied Sciences, vol. 11, no. 10, pp. 2669-2673, 2016.

[33] Mohammed Fdaili, Ahmed Essadki, and Tamou Nasser, "Comparative Analysis Between Robust SMC & Conventional PI Controllers Used in WECS Based on DFIG", International Journal of Renewable Energy Research, vol. 7, no. 4, pp.2152-2161, 2017.

[34] Ali Thaeer Hammid, Mohd Herwan Bin Sulaiman, and Ahmed N. Abdalla, "Prediction of small hydropower plant power production in Himreen Lake dam (HLD) using artificial neural network", *Alexandria Engineering Journal, 2017. (Article in press).*

[35] Othmane Zamzoum, Youness El Mourabit, Mustapha Errouha, Aziz Derouich, and Abdelaziz El Ghzizal, "Active and Reactive Power Control of Wind Turbine based on Doubly Fed Induction Generator using Adaptive Sliding Mode Approach" *International Journal of Advanced Computer Science and Applications(IJACSA)*, vol. 10 no. 2, pp.397-406, 2019.

[36] Nguyen Gia Minh Thao, Kenko chida, Kentaro Kofuji, Toru Jintsugawa, Chikashi Nakazawa, "A Comprehensive Analysis Study about Harmonic Resonances in Megawatt Grid- Connected Wind Farms", 2014 International Conference on Renewable Energy Research and Applications (ICRERA), Milwakuee, USA, pp. 387-394, 2014.

[37] E. Hamatwi, I E Davidson, M N Gitau, "Control of multi-Level Voltage Source Converters Integrating a Wind Turbine System into the Grid," 2016 *International Conference on Renewable Energy Research and Applications* (*ICRERA*), Birmingham, UK, pp.813-819, 2016